A discrete approach for modeling cell–matrix adhesions

J. Escribano · M. T. Sánchez · J. M. García-Aznar

Abstract During recent years the interaction between the extracellular matrix and the cytoskeleton of the cell has been object of numerous studies due to its importance in cell migration processes. These interactions are performed through protein clutches, known as focal adhesions. For migratory cells these focal adhesions along with force generating processes in the cytoskeleton are responsible for the formation of protrusion structures like lamellipodia or filopodia. Much is known about these structures: the different proteins that conform them, the players involved in their formation or their role in cell migration. Concretely, growth-cone filopodia structures have attracted significant attention because of their role as cell sensors of their surrounding environment and its complex behavior. On this matter, a vast myriad of mathematical models has been presented to explain its mechanical behavior. In this work, we aim to study the mechanical behavior of these structures through a discrete approach. This numerical model provides an individual analysis of the proteins involved including spatial distribution, interaction between them, and study of different phenomena, such as clutches unbinding or protein unfolding.

J. Escribano · J.M. García-Aznar (✉)
Universidad de Zaragoza, Campus Rio Ebro,
50018 Zaragoza, Spain
e-mail: jmgaraz@unizar.es

J. Escribano
e-mail: jescribs@unizar.es

M.T. Sánchez
Centro Universitario de la Defensa Zaragoza Academia General Militar,
Crta. de Huesca s/n, 50090 Zaragoza, Spain
e-mail: tererua@unizar.es

1 Introduction

Cell migration is crucial in a wide range of biological processes like chemotaxis, cancer metastasis, tissue regeneration and development. Nevertheless, despite the importance of this phenomenon, it still exists a deep unawareness of the main mechanisms that mediate this process. This lack of knowledge is due to the high variability of morphology that cells show during migration and its strong dependency on environmental factors, such as dimensionality, stiffness of the matrix and chemical gradients [29]. During migration, cells can present two different extreme main migration modes: amaeboid (weak adhesions) and mesenchymal (strong adhesions). Therefore, the understanding of cell–matrix adhesions is essential for advancing in the comprehension of cell migration. Cell adhesion is the mechanism that ensures structural integrity of tissue [39], and it is mainly regulated by mechanical processes [11,46]. Moreover, forces generated by cells are crucial in morphological tissue changes during cell migration, along with other processes such as spreading, migration and division [22,38,48]. The force generating processes in the cytoskeleton are closely related to the building of adhesion sites, called focal contacts or focal adhesions (FAs) [15,38]. These connections make the mechanical forces generated in the cytoskeleton (usually by myosin proteins) to reach the extracellular matrix (ECM), allowing the cell to sense the mechanical properties of their surroundings, which will regulate the cell behavior. Focal contacts are mainly localized in the edge of cells in like-protrusion structures such as lamellipodia and filopodia [14]. When they are found in high concentration (i.e. in these kind of structures), they are called focal adhesions. These adhesions are strongly related with the retrograde flow of the actin filaments, which is driven by actin polymerization and myosin contractility [36].
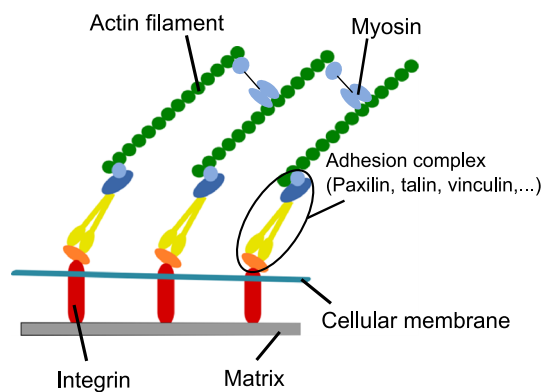
Fig. 1 Scheme representation of the main components that define the cell–matrix attachment through actin cytoskeleton

In fact, migrating cells are governed by a cycle of membrane protrusion, cell adhesion to the matrix, cytoskeleton contraction and de-adhesion at the cell rear [43]. This cyclic process in protruding lamellipodia is mainly regulated by the cell cytoskeleton through the filamentous actin (F-actin) assembly and retrograde flow (see Fig. 1). These adhesions connect the cytoskeleton of a cell to the extracellular matrix by means of a dynamic and complex set of proteins. Actually, these adhesions are implemented by transmembrane receptors from the integrin family [9] (which are placed in the cell membrane and reach both sides), binding protein ligands of the ECM, like fibronectin family [35], with the actin cytoskeleton through a clutch of proteins that include talin, α-actinin, vinculin and paxilin [39,49]. The polymerization of actin filaments provides the force for membrane deformation causing membrane protrusion. Contractile forces are generated by the myosin II, which moves antiparallel actin filaments past each other and thereby provides the force that rearranges the actin cytoskeleton [29]. Finally, these protrusions must adhere to the matrix to define cell locomotion. If they do not attach, protrusions are unproductive and tend to move rearward in waves in response to the tension generated in the cell, in a process known as membrane ruffling [4]. Therefore, actin retrograde flow is strongly dependent on cell contraction and focal adhesion size, concentration and strength [17].

In this work, we propose a discrete computational model for the simulation of the actin retrograde flow in filopodia growth-cone structures. Filopodia are found interposed along the lamellipodium leading edge and they consist of bundles of actin filaments that are packed together and protrude forward [24]. Filopodia not only play a role as adhesion sites, but also as sensors of the environment that surrounds the cell and signaling [50], and they also contain the receptors for the guidance molecules [3,25,33,42].

Mathematical modeling of cell adhesion is crucial for advancing in the understanding of how cells regulate their cytoskeleton to lead their locomotion [16]. Therefore, a high

number of conceptual [8,34] and mathematical works [2,13] have been developed to unravel how mechanical stimulus and cell-matrix properties regulate the dynamics of FAs. Most of these works are based on stochastic dynamics of multiple receptor–ligand bonds [13]. So, for example, Nicolas et al. [26] proposed that the FA mechanosensitivity can be enhanced by deformation-induced increase in the affinity of plaque proteins that form the adhesion. Shemesh et al. [40] considered FA growth as a consequence of enhanced aggregation of FA proteins in the direction of force application. Deshpande et al. [10] proposed a model of cellular contractility that accounts for dynamic reorganization of cytoskeleton. Chan and Odde [7] investigated ECM rigidity sensing of filopodia via a stochastic model of the motor-clutch force transmission system, where integrin molecules work as mechanical clutches linking F-actin to the substrate and mechanically resisting myosin-driven F-actin retrograde flow. More recently, Novikova et al. [27] proposed an original mathematical model for stiffness-sensing at focal adhesions, based on the interplay of catch-bond dynamics in the integrin layer and intracellular force generation through contractile fibers. One of the main limitations of these approaches is the assumption that total force is equally transmitted to all the bonds, not considering the spatial distribution of the focal adhesions. Another different strategy is based on a continuous approach considering energetic basis. Olberding et al. [28] proposed a theoretical treatment of focal adhesion dynamics as a nonlinear rate process governed by a classical kinetic model. Kong et al. [21] treated the focal adhesion as an adhesion cluster and studied the stability of this cluster under dynamic load by applying cyclic external strain on the substrate. There are also other works that were not specifically conceived for cell adhesions, but their methodology can be applied to model them. For example, Sauer and Wriggers [37] presented a three dimensional finite element method for contact problems developing a computational contact formulation that captures intermolecular forces such as van der Waals adhesions.

In focal adhesions sites it is important to assess the impact that protein folding phenomena has on them. In this paper, a force dependent model is implemented, but this phenomenon has been the focus of numerous numerical and mathematical studies during the last years. Thanks to technological advances in computer hardware and software, the possibilities of performing numerical analysis on this subject has increased and improved. Different numerical approaches have been developed in order to simulate protein folding, from making predictions of a folded peptide from its primary sequence to Monte Carlo simulations [23,41] or different molecular dynamics simulations [44]. For example, Monte Carlo simulations are used to obtain an approximation of a dynamically folding pathway. However, in order to understand how the mechanism of the whole folding

process is, atomistic molecular dynamics simulations are used, since they provide information about the transitions between structures [12]. The accuracy of these simulations relies on the capacity of the different physical models (force fields) to reproduce the true potential energy surfaces of proteins [6,32]. Freddolino et al. [12] analyzed the challenges that molecular dynamic simulations face, mainly due to the amount of sampling needed in order to model protein folding and the accuracy required from empirical force fields that represent the true free energy surface on which a protein folds. It is also interesting to remark the work of Waisman and Fish [47], in which they originally proposed a variant of the full approximation storage (FAS) technique [5]. This method allowed the consideration of different force fields at various scales, enhancing in that way the flexibility and the computational performance. More recently, Piana et al [32] evaluated the accuracy of the force fields typically used in folding simulations.

The binding phenomenon treated in this article has also been simulated in other numerical works. They are based on the estimation of the binding energy and different computational approaches are widely discussed in Viet's work [45]. These approaches can be divided in docking methods, where scoring functions are used to identify the most stable receptor ligand conformation, and methods based in Brownian dynamics simulations. They used conformational sampling to generate thermodynamical averages. There are a wide variety of methods used to compute the binding free energy such as linear interaction energy (LIE), linear-response approximate (LRA), molecular mechanics Poisson–Boltzmann surface area (MM-PBSA) [20] and thermodynamics integration (TI). Generally, these methods are more accurate than docking methods but, they are more time consuming.

In this work, we present a mathematical model to simulate filopodia protrusion phenomenon during the actin retrograde flow process. This model takes into account the different set of proteins involved: from myosin and actin filaments to the ligands on the ECM, including the linking proteins that perform the adhesion. Therefore, in this work we aim to understand through numerical discrete simulations how the spatiotemporal assembly, disassembly and reorganization of focal adhesions influence on the force transmission from the acto-myosin contractile system to the extracellular matrix.

2 Materials and methods

In this section we present the simulation model together with the equations that govern its behavior and the hypotheses in which it is based. The main goal of this model is to reproduce the retrograde flow of actin filaments in filopodia protrusions due to the dynamics of cell–matrix adhesions. The number of components involved in this phenomenon is considerable,

therefore some simplifications are required due to its complexity. More than 150 hundred types of proteins are involved in the linkage between the cytoskeleton and the extracellular matrix, but in this paper we only consider the effect of myosin proteins, actin filaments, extracellular ligands and protein complexes. These protein complexes, called adhesion complexes (ACs), are formed by a myriad of intracellular proteins (paxilin, vinculin, talin,…), and also by the integrins in the cell membrane [39]. These bind the actin filaments with the extracellular ligands in the matrix, addressed from now on as simply ligands.

2.1 Brief description of the simulation model

The development of a full discrete model that includes all the protein complexes and their interactions involved in the formation of a filopodium would imply a huge computational cost. Due to this, a simplification of the actual case is proposed, presenting a model that consists on a single actin filament bound to the ECM. The system movement starts when myosin proteins exert a force on the actin filament provoking its retrograde flow as it is shown in Fig. 2b. As the actin filament is driven backwards, it starts to bundle with the matrix through the ligands, which are located in the substrate of the ECM. Therefore, the ligands perform a role of anchoring points. ACs oppose to the actin filament movement by transmitting the force to the matrix causing its deformation. In this work, ACs are considered as a complex with two diferent arms (see Fig. 2a): one of them binds to the actin filament (actin-arm), and the other binds to the ECM (matrix-arm). In this model, as a first approach, the effect of the cellular membrane is not taken into account. Therefore, the actin filament is connected directly with the ligands through the ACs. The model scheme is shown in Fig. 2b.

The simulation model can be divided in three different components, where force balance is considered. In the following sections, the mathematical equations that govern the model are described.

2.2 Actin–myosin complex

We assume that the actin filament presents a solid rigid behavior and it only moves in the horizontal direction; therefore, only forces in that direction are considered. In addition, we consider that the myosins can only exert a force to pull from the actin filaments. The magnitude of this force depends on the number of myosin heads attached to the actin filament. The force exerted by the myosin heads is considered constant and equal between them. Thus, the total force is given by:

$$F_m = F_c \cdot n_m, \tag{1}$$

where F_c is the force exerted by each myosin head and n_m is the number of myosin heads attached to the filament. The
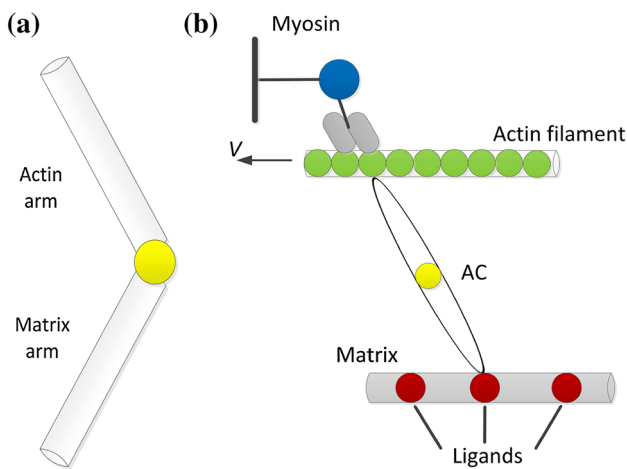
(a) **(b)**

Fig. 2 Simulation model schemes. **a** Scheme of an AC with its two arms in a non-equilibrium status. **b** Scheme of the whole simplified system proposed in this work. The actin filament is parallel to the ECM. ACs bind the actin monomers of the filament with the ligands that are fixed to the matrix

ACs bound to the actin filament oppose to that force and, as a result of the balance of these two forces, the actin filament velocity can be obtained [7]:

$$v_{filament} = v_u(1 + \frac{F_r}{F_m}), \tag{2}$$

where F_r is the force applied by the bound ACs and v_u is the actin velocity for the unloaded filament, that is, when $F_r = 0$.

2.3 Adhesion complexes (ACs)

The AC is the clutch of proteins that binds the actin filament with the extracellular matrix through the ligands. It is considered as two different bars (arms) with the same model behavior and linked between each other for one side, leaving the free one to bind with the actin filament and ligands, respectively. One arm is only capable to clutch with the actin and the other only with the ligand.

The behavior of the ACs is expressed in terms of Brownian dynamics. The equations that govern this behavior are now detailed together with the different phenomena that have been proposed for them: binding-unbinding and folding-refolding.

2.3.1 Brownian dynamics

We assume that the Langevin equation governs the dynamical behavior of the ACs [18]. Therefore, if we consider the ith AC,

$$m_i \frac{d^2\mathbf{r}_i}{dt^2} = \mathbf{F}_i - \zeta_i \frac{d\mathbf{r}_i}{dt} + \mathbf{F}_i^B, \tag{3}$$

where m_i is the mass of the AC, r_i corresponds to its current position, $\mathbf{F}_i$ are the interaction forces among proteins, ζ_i is the drag coefficient and $\mathbf{F}_i^B$ is a stochastic force. This equation allows the computation of the new position of each particle for each time increment. In addition, considering that the inertial effects of the ACs barely have an influence on the system in the considered time scale, the acceleration term in Eq. (3) can be neglected, and therefore:

$$\frac{d\mathbf{r}_i}{dt} = \frac{1}{\zeta_i}(\mathbf{F}_i^B + \mathbf{F}_i). \tag{4}$$

In order to satisfy the fluctuation-dissipation theorem, the stochastic force, $\mathbf{F}_i^B$, is chosen from a random distribution verifying the following expectation values:

$$\left\langle \mathbf{F}_i^B(t) \right\rangle = 0, \qquad \left\langle \mathbf{F}_i^B(t)\mathbf{F}_j^B(t) \right\rangle = \frac{2k_B T \zeta_i \delta_{ij}}{\Delta t}\boldsymbol{\delta}, \tag{5}$$

where k_B is the Boltzmann constant, T the absolute temperature, δ_{ij} is the Kronecker delta, $\boldsymbol{\delta}$ the second order unit tensor and Δt the time increment considered in the simulation. As a first approach, it is considered for simplicity that the geometry of the AC corresponds to a sphere, therefore the drag coefficient is:

$$\zeta_i = 3\pi\eta\sigma_i, \tag{6}$$

with σ_i being the diameter of the sphere and η the viscosity of the medium.

For the interaction forces, we consider that $F_i = F_s + F_b$, where F_s is the internal force of the AC and F_b is the force induced by the moment created for the orientation of the ACs arms respect to their balance position. Then, $F_s(r_{12})$ is given by [19]:

$$F_s(r_{12}) = \begin{cases} \frac{k_B T}{p}\left[\frac{(2l_{0,i}-r_{12}-r_0)(r_{12}-r_0)}{4l_{0,i}^2(1-r_{12}/l_{0,i})^2(1-r_0/l_{0,i})^2} + \frac{r_{12}-r_0}{l_{0,i}}\right] & \text{if } r_{12} \geq r_0, \\ k_{s,ACP}(r_{12}-r_0) & \text{if } r_{12} \leq r_0, \end{cases} \tag{7}$$

where r_{12} is the current length of the AC, r_0 is its length at rest state, p is the persistence length, $l_{0,i} = 40 + 10i$ is the maximum extension for the ith unfolding, phenomenon that will be presented in the next section.

The force induced by the orientation is given by

$$M_b = \frac{1}{2}k_b(\theta - \theta_0), \quad F_b = M_b l_{AC}, \tag{8}$$

where k_b is the bending stiffness, θ_0 is the balance orientation for the AC arms and l_{AC} is the lenght of one arm of the AC. Figure 3 shows the schemes of an AC subjected to the interacion forces F_s and F_b, respectively.
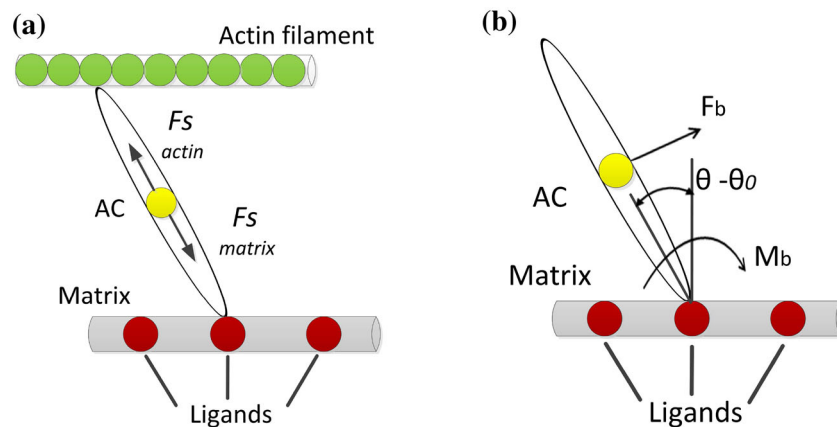
Fig. 3 Scheme of ACs subjected to different interaction forces. **a** Internal forces on ACs. Each arm is subjected to a different force depending on their own length. In the central point, the balance between these two forces is carried out and, as a consequence, the central point moves until the forces are in equilibrium. **b** Scheme of an AC subjected to the

moment created by the AC orientation respect to the balance position, M_b. This moment is applied on the central point of the AC causing its movement towards the balance position, θ_0. In this figure it is only shown an AC bound to the ligands, but the same methodology is applied when it is bound to the actin filament

2.3.2 Unfolding/refolding

Experimental tests show that some proteins such as fribonectin or actin crosslinkers can sustain unfolding under determined extensional forces [1,19]. In this work, we assume that the ACs present a similar behavior. Therefore, the internal force–extension curve of the AC exhibits a sawtooth behavior; this curve presents peak values around 30 pN, at 10 nm intervals (see Fig. 4). Then, unfolding phenomena is regulated by the unfolding rate, k_{uf} [19]:

$$k_{uf} = \begin{cases} k_{uf}^0 exp(\frac{\lambda_{uf} F_s}{k_B T}) & \text{if } r_{12} \geq r_0, \\ 0 & \text{if } r_{12} \leq r_0, \end{cases} \tag{9}$$

where λ_{ub} is the mechanical compliance, k_{ub}^0 is the zero-force unfolding rate coefficient and F_s is the internal force of the AC seen in previous section, Eq. 7.

When unfolding happens, it exists the possibility that the inverse phenomenon occurs, phenomenon known as refolding. This happens when the AC shrinks below the length at which the last unfolding occured, then ith unfolding decreases by 1.

Finally, k_{uf} corresponds to the rate parameter of an exponential distribution function, therefore the probability of the event is:

$$P = 1 - e^{k_{uf} \Delta t}. \tag{10}$$

2.3.3 Binding/unbinding

ACs present the possibility of separating from the actin filament or the ligands when they are bound to them. This phenomenon is similar to the unfolding one, and it is governed by the unbinding rate, k_{ub} [19]:
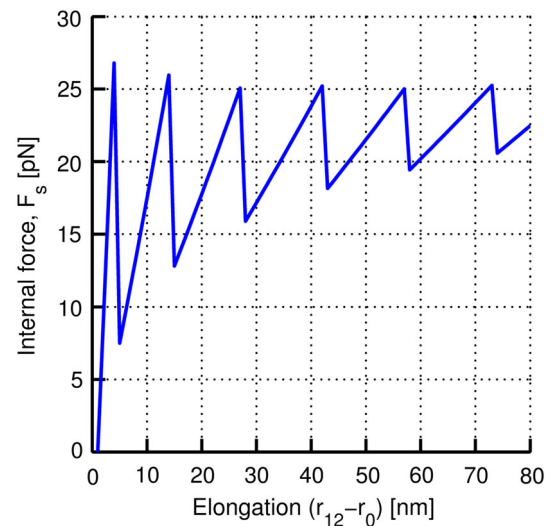

Fig. 4 Internal force of an AC arm against its elongation. The sawtooth behavior is clearly observed: when the force reach values around 30 pN, unfolding occurs. This provokes a reduction in the internal force for the same arm elongation

$$k_{ub} = \begin{cases} k_{ub}^0 exp(\frac{\lambda_{ub} F_s}{k_B T}) & \text{if } r_{12} \geq r_0, \\ 0 & \text{if } r_{12} \leq r_0, \end{cases} \tag{11}$$

where λ_{ub} is the mechanical compliance of the bond in the unbinding case and k_{ub}^0 is the zero-force unbinding coefficient. In this model, when unbinding occurs, both arms of the AC refold completely and return to their rest state ($r_{12} = r_0$). The probability of this event is given by an exponential distribution function, similar to Eq. 10.

Free ACs can also bind to the actin filament or the ligands. This process is determined by the distance between them, occurring when

Fig. 5 Flow chart of the implemented algorithm
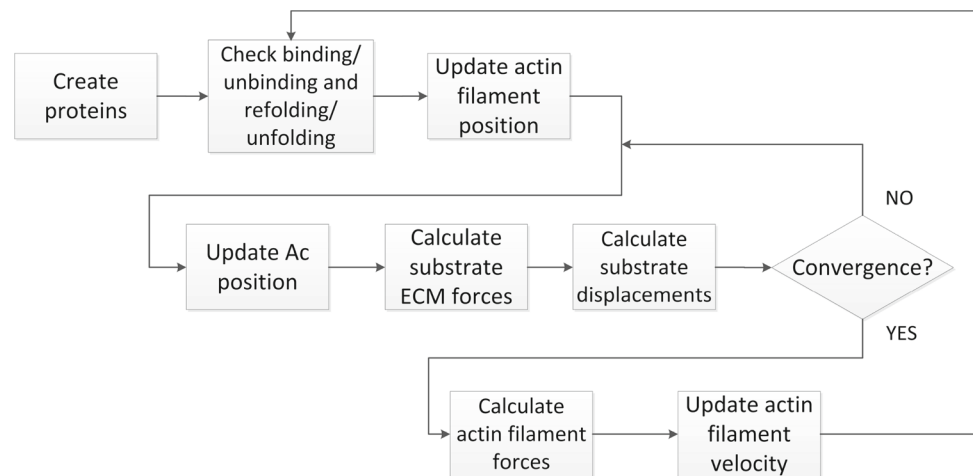
$$d_{12} \leq 2^{1/6}\sigma_{12}, \tag{12}$$

d_{12} being the distance between the two particles and σ_{12} the average diameter of both particles.

2.4 The extracelullar matrix (ECM)

The extracellular matrix is considered as a set of truss elements, which only bears axial forces. Therefore, its behavior can be explained in terms of the global stiffness matrix

$$F_{str} = K_{str}U_{str}, \tag{13}$$

where F_{str} is the force vector, K_{str} is the stiffness matrix of the ECM and U_{str} is the displacement vector corresponding to all their ligands.

The values of the stiffness matrix depends on the product of the elastic modulus of the ECM, E, and its surface area, A. For this work, we consider that A presents a fixed value and we only change the value of E for all the simulations. We also assume that in each node the discretization of the elements is occupied by one ligand. Hence, the force vector is obtained from the forces exerted by the ACs on each ligand, and the displacement vector is applied on them. Initially, as a first approach, we are working under the assumption of small strains and displacements. Therefore, we assume a linear elastic behavior for the ECM and K_{str} remains constant.

3 Numerical implementation

In this section, an explicit algorithm is proposed to implement all the equations seen in the previous section, based on the following steps: First, given the initial conditions, an analysis of the current position of the ACs, actin monomers and ligands is performed in order to check the different phenomena considered (binding–unbinding and unfolding-refolding). Next,

the actin filament moves, and as a consequence, the force balance in the system breaks the mechanical equilibrium. This provokes ACs and ECM deformation, requiring an iterative process to reach the force balance again. Finally, the new force on the actin filament is calculated and therefore its velocity is obtained.

As a first approach, we consider that the actin filament polymerizes by setting one actin monomer after another creating in that way a straight filament. The ECM is considered parallel to the actin filament with the ligands distributed on it with a random distribution. The ACs are placed randomly in the spatial domain set for the simulation. Both actin and ligands are considered as particles and they are defined only by their central point. Nevertheless, although the ACs are also considered as particles when random movement, they are defined by three points and behave like two attached arms for the rest of scenarios. From now on, these three points are known as: AC-actin point, that binds the AC with the actin monomers in the filament and corresponds to the edge of the actin-arm; AC-matrix point, which corresponds to the edge of the matrix-arm and binds to ligands; and AC-central point that corresponds to the point where both arms intersect.

3.1 Development of the algorithm

We present an algorithm for the spatiotemporal resolution of this problem, which is solved in a discrete form, for each time increment, n. The algorithm is schematically shown in Fig. 5, and it is mainly based on three balances of forces.

The whole system mechanism starts by creating the different components involved as it was explained before. Next, the iteration process begins. Firstly, an analysis of the current situation of the different proteins involved in the system is carried out. This let the algorithm know if some protein binding phenomenon is occurring. If an AC-actin point is sufficiently close to a free actin monomer, they automatically clutch. The same process occurs with the ligands and

the AC-matrix points. Then, the algorithm separates the ACs in four different scenarios depending on their linkage:

- *Case 0* Fully free. The ACs moves randomly in the medium.
- *Case 1* Bound to actin filament. The entire AC moves with the actin filament in its balanced position.
- *Case 2* Bound to matrix. The entire AC moves with the matrix in its balanced position.
- *Case 3* Fully bound to actin filament and to matrix. The AC is deformed under the effect of the actin movement and the resistance that the matrix exerts to it.

For the ACs in Case 3, the unbinding and unfolding-refolding phenomena are studied. Firstly, refolding is checked, that is, when the AC arm has shrink below the length at which the last unfolding occurs. If there is no refolding, then the unfolding phenomenon is studied as it was explained in the mathematical model. After, the unbinding is checked. All these analysis are carried out in both arms of the AC.

Next, the actin filament is moved, modifying its position. The AC-actin points attached to the filament move with it (Case 1 and Case 3), elongating the ACs actin-arm and breaking the force balance of the system. It is important to remark that the actin filament only moves in horizontal direction.

Due to this, a force balance in the matrix is evaluated. An iterative process starts and it is repeated until the equilibrium is fulfilled. The matrix balance begins by performing a local force balance in each AC of Case 3. This local force balance consists of an internal iterative process. Internal forces (Eq. 7) are calculated for both arms of the ACs and their AC-central points are moved as a result, following Eq. 4. When the difference between the two forces is below a threshold, the AC is in balance again and therefore the internal iterative process ends. After all the ACs are in equilibrium, the forces over the ECM are calculated. These forces correspond to the ones exerted by the AC matrix-arm over the ligands. Once these forces are known, the ECM displacements are calculated by using the stiffness matrix (Eq. 13). When the matrix is deformed, the AC-matrix point moves with it, causing the elongation of the matrix-arm if the AC is in Case 3, or just a displacement, if it is in Case 2. This process breaks again the internal force balance of the AC, so it is necessary to recalculate the AC force balance, the force vector and the new displacements. This process is repeated until the displacements are lower than a threshold. It also exists the possibility that the increment of the ligand displacements diverges. In that case the loop is restarted recovering the initial values, and the time increment is divided by two.

Once the matrix balance is achieved the forces exerted by the AC over the actin filament are calculated. Finally, the new actin filament velocity is computed through Eq. 2 and a new time iteration starts.

4 Numerical simulations: reference cases

In order to evaluate the potential of the model, several simulations are conducted. The aim of these simulations is to asses the influence of the ECM stiffness on the actin retrograde flow velocity and its effect on the adhesion size and on the traction forces. The values of the parameters used in the model are shown in Table 1. The exact values of the mechanical properties of the ACs and some parameters related to unbinding and unfolding phenomena are yet unknown, therefore, we have estimated their values in order to simulate this experiment.

As mentioned in previous sections, we have designed a discrete algorithm to model the retrograde flow of the actin filament and to study the effect of the CAs in the process. The results shown in this section corresponds to nine seconds of simulation and the actin velocity is computed as the average value of the 6 last seconds of simulation (for the cases where a velocity analysis is considered), in order to show the velocity when the system is already stabilized and not when the clutches are being created and the randomness of the system is considerable. The results obtained for the initial values of the variables shown in Table 2 can be seen in Fig. 9. For a soft matrix, the actin speed is almost maximum, but as the stiffness increases, the actin speed starts to decrease. The velocity keeps decreasing until it reaches a point and, after it, the speed abruptly increases again to almost maximum values. A similar tendency has been observed in some experimental results [7].

This kind of behavior can be justified from our simulations. When the matrix is very soft, it can be deformed by minimum forces (considerably lower than the ones exerted by the myosin), so it moves along with the actin. The fully bound ACs move with them, almost without deforming. When the matrix stiffness increases, the matrix deforms slower exerting gradually more force to oppose to the actin filament movement. Due to this, the ACs are subjected to an increasing elongation and, therefore, to an increasing stress to bear. The abrupt increment in the speed occurs when the matrix is not able to deform enough due to its high stiffness and the elongation of the ACs leads to the adhesion failure. As the ACs start to disengage, the force required to remain the others bound increases, accelerating in this way the unbinding process. Therefore, in a short period of time, all the ACs are found unbound. In order to see clearly these three kind of behaviors, we have reproduced the state of each component at the following time steps: 0 s (initial), 3 s, 6 s and 9 s (end). The results are shown in Figs. 6, 7 and 8 for soft, intermediate and stiff matrix, respectively.

It has also been experimentally observed that the traction forces that the matrix exerts increase with the size of the adhesion [38]. In Fig. 10, this behavior is reproduced for different matrix stiffness. As the adhesion grows, more ACs are conforming the union between actin filament and matrix; there-

Table 1 Numerical values for the mechanical data and phenomena parameters

Parameter	Symbol	Value	Source
Myosin head force	F_c	-2 (pN)	[7]
Unloaded actin filament velocity	v_u	-120 (μm/s)	[7]
AC balance length	r_0	30 (nm)	Estimated
AC arm length	L_{AC}	30 (nm)	Estimated
Boltzman energy	$k_B T$	4.142×10^{-21} (J)	[18]
AC stiffness against compression below the equilibrium length	$k_{(s,AC)}$	4.23×10^{-5} (N/m)	Estimated
Zero-force unfolding rate coefficient	k_{uf}^0	3×10^{-5} (s^{-1})	[19]
Mechanical compliance for the actin arm	$\lambda_{uf,actin}$	1.442 (nm)	Estimated
Mechanical compliance for the matrix arm	$\lambda_{uf,matrix}$	2.884 (nm)	Estimated
Zero-force unbinding rate coefficient	k_{ub}^0	0.115 (s^{-1})	[19]
Mechanical compliance of the actin bond for unbinding	$\lambda_{ub,actin}$	0.25 (nm)	Estimated
Mechanical compliance of the matrix bond for unbinding	$\lambda_{ub,matrix}$	0.5 (nm)	Estimated
Persistence length for the actin arm	p_{actin}	0.04 (nm)	Estimated
Persistence length for the matrix arm	p_{matrix}	0.04 (nm)	Estimated
Maximum number of unfolding for the marix-arm	n_{uf}	2	Estimated
Simulation step time	Δt	0.003 (s)	Estimated
Total time of the simulation	t	9 (s)	Estimated
Actin monomer diameter	σ_A	7 (nm)	[18]
Ligand diameter	σ_L	7 (nm)	Estimated
Medium viscosity	η	8.599×10^{-4} (kg/m s)	[18]
Bending stiffness	k_b	15.74 (nN nm)	Estimated
Balance orientation for the AC arms	θ_0	$\pi/2$ (rad)	
Matrix surface	A	2×10^{-4} (nm^2)	Estimated

Table 2 Reference value and values for the sensitivity analysis of the initial conditions

Parameter	Ref. value	Sensitivity analysis
Ligands concentration	40	20–60–80
Number of myosin heads	75	45–60–90
Number of actin monomers	60	20–40–80 (nm)

fore, the force on the ECM also increases. In stiffer matrix, the relation is more linear since the ACs quickly disengage as the traction forces increase in the ECM. For intermediate matrix compliance, the clutches starts to build as the traction force increases slowly, but it reaches a point where the adhesion cannot grow more because of the actin filament length and it remains constant as the traction force keeps increasing.

5 Sensitivity analysis

To a better understanding of the mechanical behavior of our approach, it is important to analyze the influence that some of the components might have on it. For this purpose, a sensitivity analysis has been carried out, varying some parameters that are crucial for understanding the role of cell–matrix

adhesions. For this analysis, we consider a random spatial distribution of the ligands. The variables subjected to analysis are shown in Table 2.

5.1 Effect of the ligand concentration

Initially, we analyze the role of the concentration of ligands. The results for a concentration of 20, 40, 60 and 80 ligands are shown in Fig. 11. The ligands have been located randomly in a surface that occupies a 40 percent longer than the actin filament length. Ligands are anchoring points with the matrix, therefore a lack of these elements would drive to a weaker adhesion. When the number of ACs linking actin filament and ECM decreases, the force that holds the actin filament decreases as well. For the same reason, the stiffness at which the ACs start to disengage (provoking the filament speed to rise) decreases with the number of ligands too.

5.2 Impact of the actin filament length

The actin filament length is related with polymerization and depolymerization processes, hence it is a variable subjected to considerable changes and it is worth to study. As the fil-

Fig. 6 Simulation results for soft matrix (actin *green*; ACs *yellow*; matrix *red*; ligands *red points*). The actin filament starts to move as a consequence of the myosin action. The ACs are moving around the medium until they get close to an actin monomer or a ligand and bind to them. When they are bound to both of them they start to transmit forces to the matrix. Since the matrix is very soft it deforms very easily, moving almost at the same velocity that the actin filament and avoiding the ACs to bear big forces. (Color figure online)
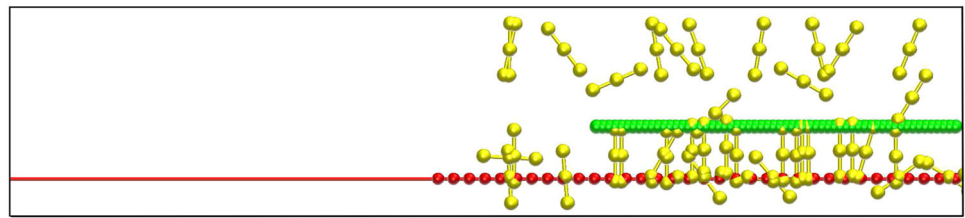
(a) Simulation time=0s
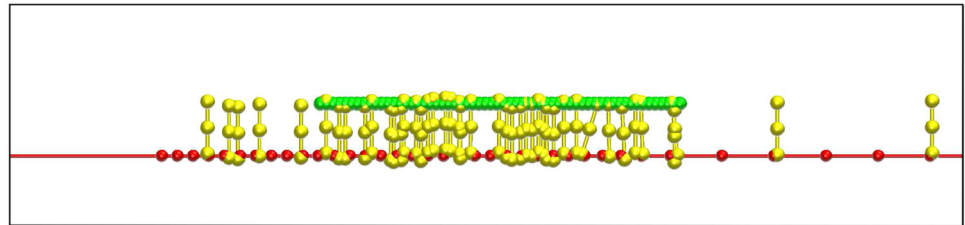
(b) Simulation time=3s
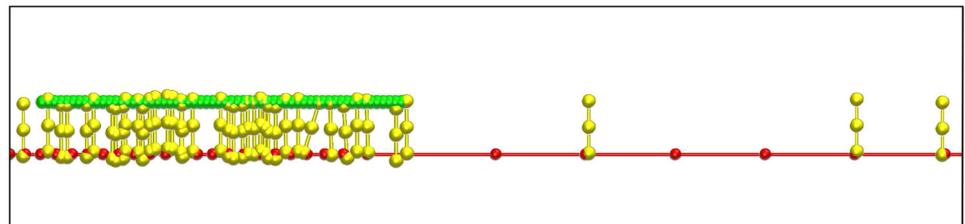
(c) Simulation time=6s
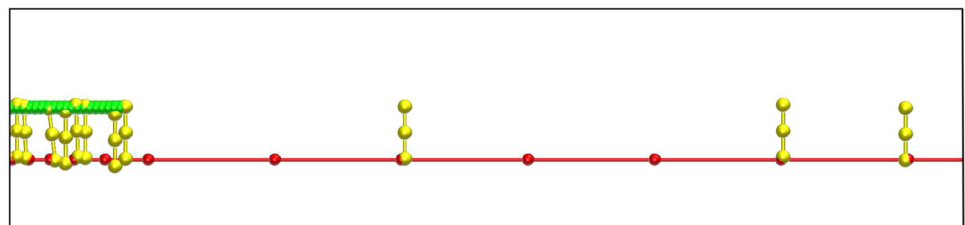
(d) Simulation time=9s

ament length increases more ACs are capable of creating bounds, provoking the linkage to grow stronger and increasing its life time. Moreover, not only new ACs have more possibilities to bind, but also the ones that were bound and at some point broke that union have more chances to re-bind. Consequently, this behavior causes a reduction in the actin filament retrograde speed. In Fig. 12 the effect on this variable is observed for actin filaments composed of 20, 40, 60 and 80 actin monomers. When more monomers are added to the actin filament, its velocity decreases considerably and a stiffer matrix is required to reach the point of minimum velocity.

5.3 Influence of the myosin traction force

Finally, the influence of the force exerted by the myosins to pull from the actin filament is analyzed. To do this, the number of myosin heads is changed in order to reproduce this effect. Each myosin head exerts a constant force to pull from the actin filament, therefore as the number of myosin heads rises the pulling force increases in a linear relation too. Results are shown in Fig. 13 for 45, 60, 75 and 90 myosin heads. As expected, when the force exerted by the myosins to pull from the actin filament increases, the actin filament velocity increases as well.

6 Conclusions and discussion

A significant amount of conceptual works regarding focal adhesions have been carried out during the last few years. Generally, they can be divided into two different groups: theoretical and numerical studies. The first ones set the basics used in the numerical ones, which, at the same time, provide

Fig. 7 Simulation results for intermediate compliance matrix (actin *green*; ACs *yellow*; matrix *red*; ligands *red points*). The matrix deforms as a consequence of the force transmitted from the actin filament through the ACs. Since the stiffness is considerable, the matrix deformation is slower than the actin filament movement causing the ACs deformation. This provokes the unbinding phenomenon on some of the ACs and the reduction on the actin filament velocity. (Color figure online)
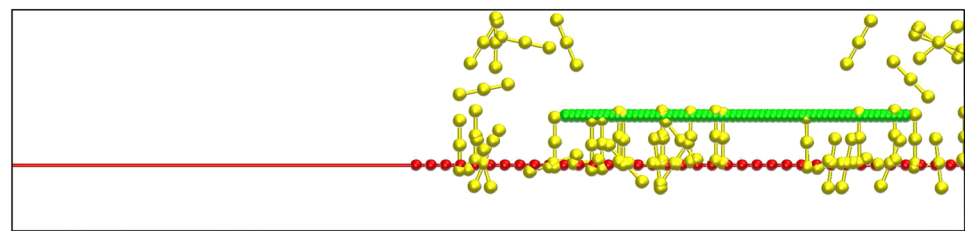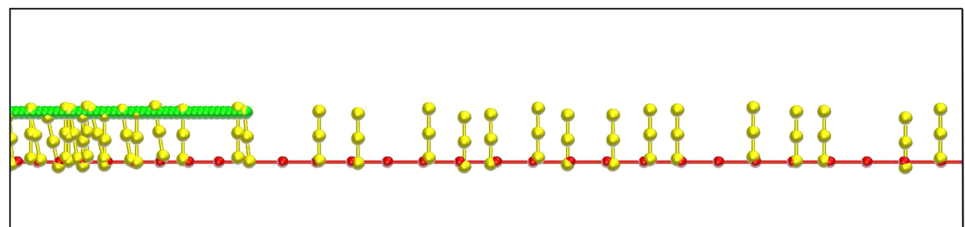

(a) Simulation time=0s
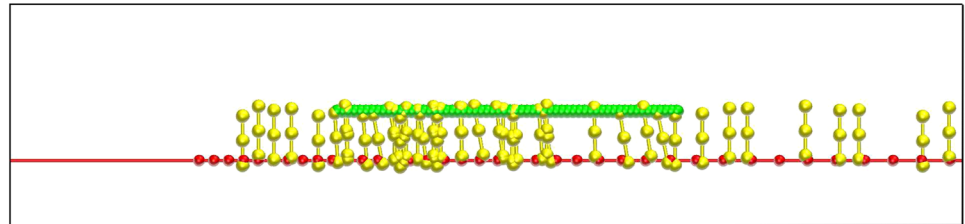
(b) Simulation time=3s
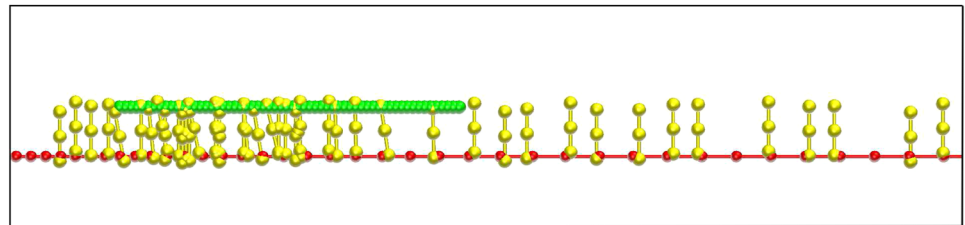
(c) Simulation time=6s

(d) Simulation time=9s

a deeper insight of the phenomena, allowing to improve theoretical models. Consequently, it emerges an enriching feedback process from which both sides get benefits. In addition, numerical models can be classified in continuous or discrete. In this work, we have developed a discrete model, since they offer the possibility of incorporating individual behavior at each complex of proteins involved in the biological phenomenon. We have provided for an insight view of these types of adhesions, that let improve our understanding of how each component individually behaves and how it interacts with the other ones that surrounds them.

In this work, we have presented a discrete algorithm to model the cell-matrix adhesions. We have shown that this discrete model is consistent with experimental data from the literature [7,38], and it presents a new approach to simulate this phenomenon. Hence, we have considered that ACs are flexible elements with a non-linear behavior and with

some important properties, such as binding–unbinding or unfolding-refolding. We have also considered the spatial distribution of the ligands on the ECM, that determines the pattern of how the traction forces are transmitted to the matrix. This model offers the possibility of analyzing, individually, the influence of the different proteins involved in the mechano-biological process: myosins in their role of traction motors or the length of the actin filament, which is constantly changing because of the polymerization and depolymerization processes. It also considers the ligand concentration in the ECM, which determines the location of the adhesions and their size .

It is fair to say that, in spite of the considerable quantity of parameters and different phenomena analyzed, there are still a great amount of factors that has not been taken into account in this model. This is due to the implicit need of establishing some simplifications in the quantity of ele-

Fig. 8 Simulation results for stiff matrix (actin *green*; ACs *yellow*; matrix *red*; ligands *red points*). The matrix stiffness is very high, therefore it barely deforms under the force transmitted by the ACs. Hence, the ACs have to bear all that force, deforming at high velocity. This provokes the rupture of the bounds and the dead of the adhesion, causing the free movement of the actin filament. (Color figure online)
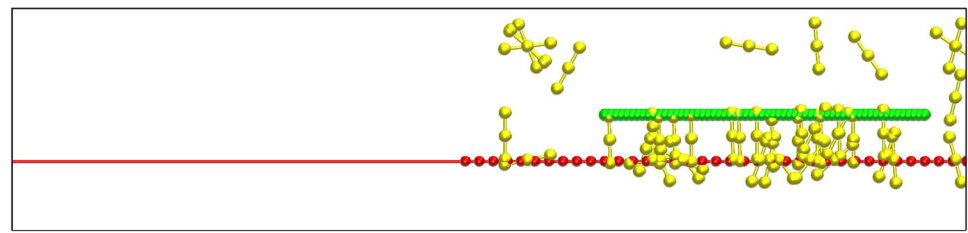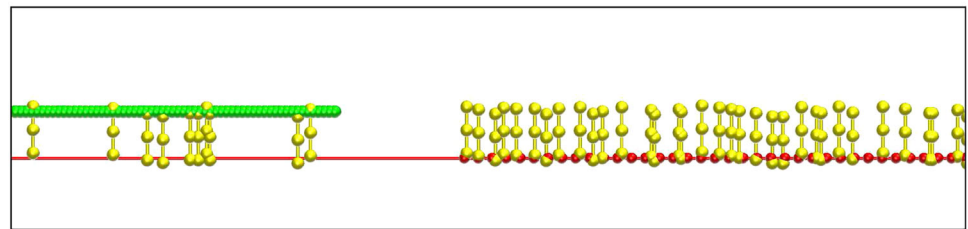

(a) Simulation time=0s
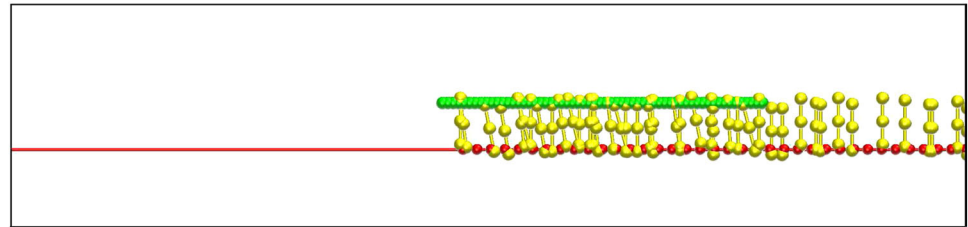
(b) Simulation time=3s
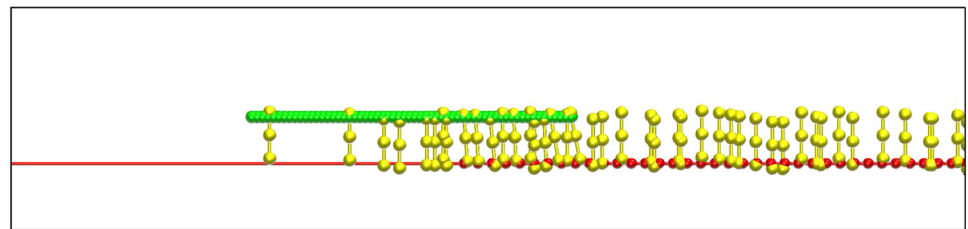
(c) Simulation time=6s

(d) Simulation time=9s

ments considered, or the need of formulating some hypothesis due to the lack of information produced by the deep unawareness that still exists about these biological processes. For example, the ACs are formed by a myriad of different proteins, but for this work, they are simplified to two main protein complexes. In addition, we have not considered implicitly the effect of the integrin proteins and the cell membrane. To conclude, the discrete modeling here presented is a relevant tool to improve the understanding of cell matrix-adhesions and to go deeper on the biological knowledge of these processes.

The next step for this kind of models is their implementation in 3D simulations. Nowadays, cell–matrix adhesions on 3D environments are being the focus of a growing number of studies and experiments, and, in order to conduct reliable simulations of them, the development of 3D models is essential. However, this work presents a considerable challenge. Besides the inherent computational cost of this kind of analyses, the mechanisms that regulate 3D cell migration remain poorly understood. It is known that the way of cell migration changes between 2D and 3D environment, but it also appears that in a 3D environment cells of the same type migrate in different ways depending on the physical properties of the extracellular matrix, the degree of extracellular proteolysis and on soluble signaling factors [30,31]. Therefore, it seems clear, that the key, in order to develop more complex and reliable models in 3D, lies on the incorporation of quantitative exper-
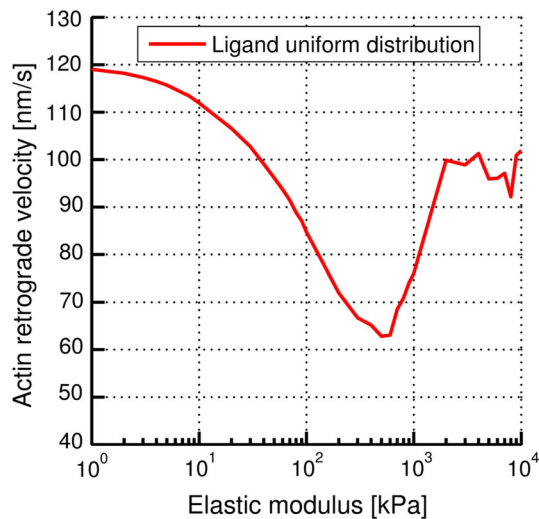
Fig. 9 Actin retrograde velocity under different ECM stiffness for a uniform distribution of ligands. For a soft matrix, the ACs deform without almost opposing to the actin filament movement. The matrix moves along with the actin filament. As the matrix stiffness increases, its deformation becomes slower, and the ACs that conform the linkage starts to elongate and to transmit the reaction force from the matrix to the actin filament. Hence, a reduction in the actin retrograde flow speed is produced. This behavior continues until the velocity reaches a minimum, 7×10^2 KPa. After that point, the ACs cannot bear the stress and start to quickly disengage, provoking a considerable increment on the actin speed

Fig. 11 Actin retrograde velocity under different matrix stiffness for different ligands concentration. When the concentration of ligands decreases to 20, the actin retrograde velocity is higher. On the contrary, when it increases to 60, the velocity decrease as a consequence of the formation of more clutches. When the concentration is equal to 80, there is no further decrease of the velocity. This is due to a saturation of ligands on the matrix and therefore, the ACs are not able to clutch with them
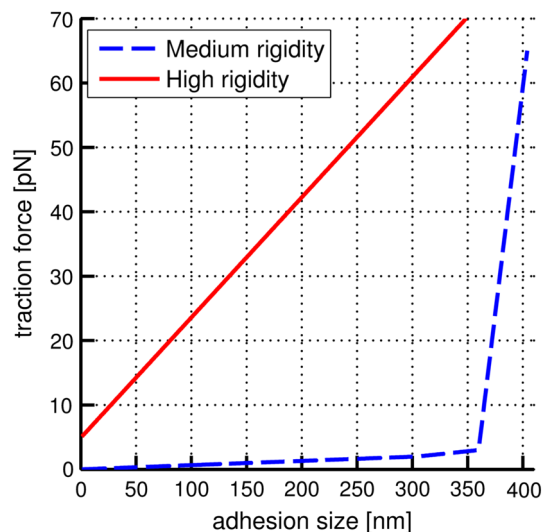

Fig. 10 Dependence of the adhesion size respect to actin retrograde speed. The more ACs are conforming the adhesion or the bigger the adhesion is, the bigger the traction force is. In intermediate compliance matrix the clutches starts to grow as the traction force increases slowly, but there is point at which the adhesion cannot grow further. The actin filament, limited by its own length, cannot host more clutches. At this point the size of the adhesion remains constant as the traction force keeps increasing. In stiffer matrix, the relation is almost linear since the ACs quickly disengage when the traction forces grows in the matrix
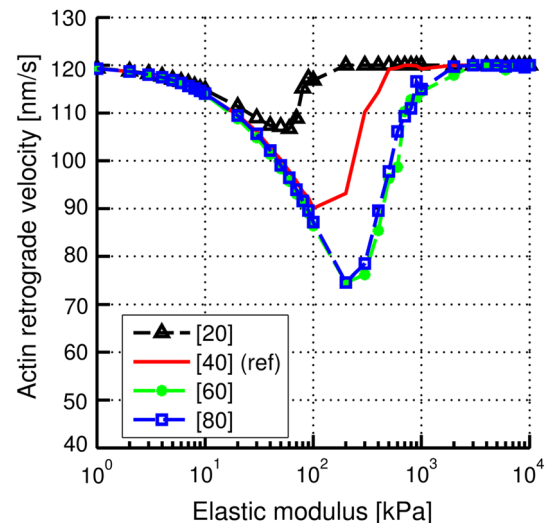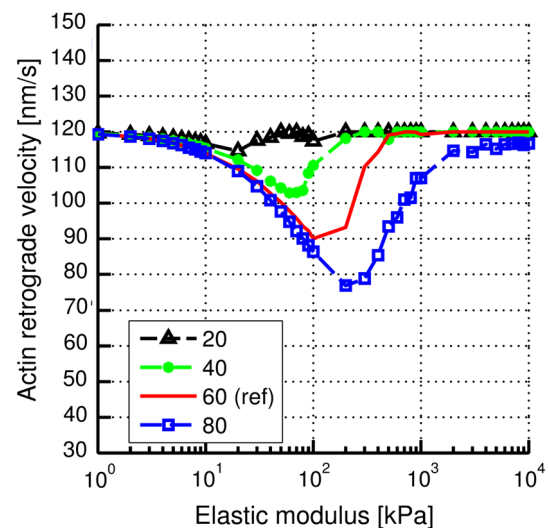

Fig. 12 Actin retrograde velocity under different matrix stiffness for different actin filament length. For a short actin filament of 20 actin monomers, few adhesion can grow, and therefore, it barely exists an opposition to the actin filament movement. When the actin filament increases to 40 actin monomers, the adhesion starts to grow stronger, provoking a velocity drop. This phenomenon continues when the actin filament grows to 60 and 80 actin monomers, being its effect clearly noticed on the corresponding curves
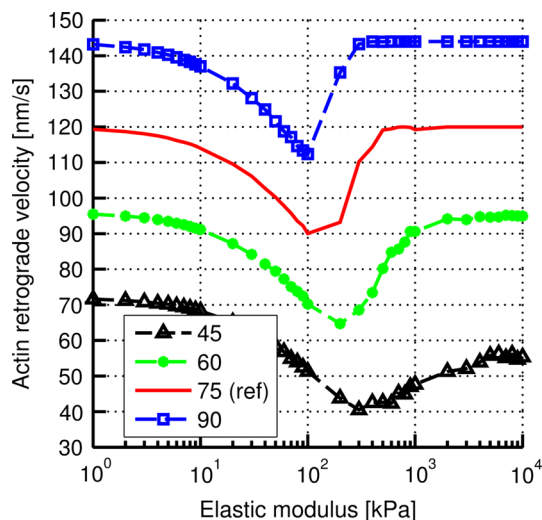
Fig. 13 Actin retrograde velocity under different matrix stiffness for different myosin traction force values. The myosin heads determines the force exerted to pull from the actin filament. When the number of myosin heads is low, 45, the actin retrograde flow speed decreases. When the number of myosin heads increases, the actin filament is driven backwards with a stronger force. This effect is observed for 60, 75 and 90 myosin heads. It can also be noticed that, the minimum velocity point for each case occurs at lower stiffness for higher number of myosin heads

imental data that could clarify the mechanism of these processes.

References

1. Bao G (2002) Mechanics of biomolecules. J Mech Phys Solids 50(11):2237–2274. doi:10.1016/S0022-5096(02)00035-2
2. Bausch AR, Schwarz US (2013) Cellular mechanosensing: sharing the force. Nat Mater 12(11):948–949. doi:10.1038/nmat3791
3. Bechara A, Nawabi H, Moret F, Yaron A, Weaver E, Bozon M, Abouzid K, Guan JL, Tessier-Lavigne M, Lemmon V, Castellani V (2008) FAK-MAPK-dependent adhesion disassembly downstream of L1 contributes to semaphorin3A-induced collapse. EMBO J 27(11):1549–1562. doi:10.1038/emboj.2008.86
4. Borm B, Requardt RP, Herzog V, Kirfel G (2005) Membrane ruffles in cell migration: indicators of inefficient lamellipodia adhesion and compartments of actin filament reorganization. Exp Cell Res 302(1):83–95. doi:10.1016/j.yexcr.2004.08.034
5. Brandt A (1977) Multi-Level adaptive solutions to boundary-value problems. Math Comput 31(138):333. doi:10.2307/2006422
6. Caflisch A, Paci E (2005) Molecular dynamics simulations to study protein folding and unfolding. In: Buchner J, Kiefhaber T (eds) Protein folding handbook, vol 05. Wiley-VCH, Weinheim, pp 1143–1169
7. Chan CE, Odde DJ (2008) Traction dynamics of filopodia on compliant substrates. Science 322:1687–1691 (New York)
8. Choi CK, Vicente-manzanares M, Zareno J, Leanna A, Mogilner A, Horwitz AR, Engineering B (2008) Actin and α-actinin orchestrate the assembly and maturation of nascent adhesions in a myosin II motor-independent manner. Nat Cell Biol 10(9):1039–1050
9. Critchley DR (2000) Focal adhesions—the cytoskeletal connection. Curr Opin Cell Biol 12(1):133–139
10. Deshpande V, Mrksich M, Mcmeeking R, Evans A (2008) A biomechanical model for coupling cell contractility with focal adhesion formation. J Mech Phys Solids 56(4):1484–1510. doi:10.1016/j.jmps.2007.08.006
11. Discher DE, Janmey P, Wang YL (2005) Tissue cells feel and respond to the stiffness of their substrate. Science 310(5751):1139–1143. doi:10.1126/science.1116995 (New York)
12. Freddolino PL, Christopher B Harrison YL, Schulten K (2010) Challenges in protein folding simulations: timescale, representation, and analysis Peter. Nat Phys 6(10):751–758
13. Gao H, Qian J, Chen B (2011) Probing mechanical principles of focal contacts in cell–matrix adhesion with a coupled stochastic–elastic modelling framework. J R Soc Interface 8(62):1217–1232. doi:10.1098/rsif.2011.0157
14. Geiger B, Bershadsky A, Pankov R, Yamada KM, Correspondence BG (2001) Transmembrane extracellular matrix-cytoskeleton crosstalk. Nat Rev Mol Cell Biol 2(November):793–805
15. Geiger B, Spatz JP, Bershadsky AD (2009) Environmental sensing through focal adhesions. Nat Rev Mol Cell Biol 10(1):21–33. doi:10.1038/nrm2593
16. Gerisch A, Painter KJ (2010) Mathematical modelling of cell adhesion and its applications to developmental biology and cancer invasion. In: Chauvière A, Preziosi L, Verdier C (eds) Cell mechanics: from single scale-based models to multiscale modeling, vol 2, chap 12. Chapman and Hall/CRC, USA pp 319–350
17. Kim DH, Wirtz D (2013) Focal adhesion size uniquely predicts cell migration. FASEB Journal 27(4):1351–1361. doi:10.1096/fj.12-220160
18. Kim T, Hwang W, Kamm RD (2007) Computational analysis of a cross-linked actin-like network. Exp Mech 49(1):91–104. doi:10.1007/s11340-007-9091-3
19. Kim T, Hwang W, Kamm RD (2011) Dynamic role of cross-linking proteins in actin rheology. Biophys J 101(7):1597–1603. doi:10.1016/j.bpj.2011.08.033
20. Kollman Pa, Massova I, Reyes C, Kuhn B, Huo S, Chong L, Lee M, Lee T, Duan Y, Wang W, Donini O, Cieplak P, Srinivasan J, Case DA, Cheatham TE (2000) Calculating structures and free energies of complex molecules: combining molecular mechanics and continuum models. Acc Chem Res 33(12):889–897
21. Kong D, Ji B, Dai L (2008) Stability of adhesion clusters and cell reorientation under lateral cyclic tension. Biophys J 95(8):4034–4044. doi:10.1529/biophysj.108.131342
22. Lecuit T, Lenne PF (2007) Cell surface mechanics and the control of cell shape, tissue patterns and morphogenesis. Nat Rev Mol Cell Biol 8(8):633–644. doi:10.1038/nrm2222
23. Lutz B, Faber M, Verma A, Klumpp S, Schug A (2013) Differences between cotranscriptional and free riboswitch folding. Nucleic Acids Res 1:1–10
24. Mogilner A, Rubinstein B (2005) The physics of filopodial protrusion. Biophys J 89(2):782–795. doi:10.1529/biophysj.104.056515
25. Nawabi H, Briançon-Marjollet A, Clark C, Sanyas I, Takamatsu H, Okuno T, Kumanogoh A, Bozon M, Takeshima K, Yoshida Y, Moret F, Abouzid K, Castellani V (2010) A midline switch of receptor processing regulates commissural axon guidance in vertebrates. Genes Dev 24(4):396–410. doi:10.1101/gad.542510
26. Nicolas A, Geiger B, Safran SA (2004) Cell mechanosensitivity controls the anisotropy of focal adhesions. PNAS 101(34):12,520–12,525
27. Novikova EA, Storm C (2013) Contractile fibers and catch-bond clusters: a biological force sensor? Biophys J 105(6):1336–1345. doi:10.1016/j.bpj.2013.07.039

28. Olberding JE, Thouless MD, Arruda EM (2010) The non-equilibrium thermodynamics and kinetics of focal adhesion dynamics. PloS One 5(8):e12,043. doi:10.1371/journal.pone.0012043

29. Parsons JT, Horwitz AR, Schwartz MA (2010) Cell adhesion: integrating cytoskeletal dynamics and cellular tension. Nat Rev Mol Cell Biol 11(9):633–643. doi:10.1038/nrm2957

30. Petrie RJ, Gavara N, Chadwick RS, Yamada KM (2012) Nonpolarized signaling reveals two distinct modes of 3D cell migration. J Cell Biol 197(3):439–455. doi:10.1083/jcb.201201124

31. Petrie RJ, Yamada KM (2012) At the leading edge of three-dimensional cell migration. J Cell Sci 125(Pt 24):5917–5926. doi:10.1242/jcs.093732

32. Piana S, Klepeis JL, Shaw DE (2014) Assessing the accuracy of physical models used in protein-folding simulations: quantitative evidence from long molecular dynamics simulations. Curr Opin Struct Biol 24:98–105

33. Ren XR, Ming GL, Xie Y, Hong Y, Sun DM, Zhao ZQ, Feng Z, Wang Q, Shim S, Chen ZF, Song HJ, Mei L, Xiong WC (2004) Focal adhesion kinase in netrin-1 signaling. Nat Neurosci 7(11):1204–1212. doi:10.1038/nn1330

34. Roca-Cusachs P, Iskratsch T, Sheetz MP (2012) Finding the weakest link: exploring integrin-mediated mechanical molecular pathways. J Cell Sci 125(Pt 13):3025–3038. doi:10.1242/jcs.095794

35. Ruoslahti E (1996) RGD and other recognition sequences for integrins. Ann Rev Cell Dev Biol 12:697–715. doi:10.1146/annurev.cellbio.12.1.697

36. Sabass B, Schwarz US (2010) Modeling cytoskeletal flow over adhesion sites: competition between stochastic bond dynamics and intracellular relaxation. J Phys Conden Matter 22(19):194,112

37. Sauer RA, Wriggers P (2009) Formulation and analysis of a three-dimensional finite element implementation for adhesive contact at the nanoscale. Comput Methods Appl Mech Eng 198(49——52):3871–3883

38. Schwarz US, Gardel ML (2012) United we stand: integrating the actin cytoskeleton and cell–matrix adhesions in cellular mechanotransduction. J Cell Sci 125(Pt 13):3051–3060. doi:10.1242/jcs.093716

39. Selhuber-Unkel C, Erdmann T, López-García M, Kessler H, Schwarz US, Spatz JP (2010) Cell adhesion strength is controlled by intermolecular spacing of adhesion receptors. Biophys J 98(4):543–551. doi:10.1016/j.bpj.2009.11.001

40. Shemesh T, Geiger B, Bershadsky AD, Kozlov MM (2005) Focal adhesions as mechanosensors: a physical mechanism. Proc Natl Acad Sci USA 102(35):12,383–12,388. doi:10.1073/pnas.0500254102

41. Soler MA, Faísca PFN (2013) Effects of knots on protein folding properties. PloS One 8(9):e74,755. doi:10.1371/journal.pone.0074755

42. Steketee MB, Tosney KW (2002) Three functionally distinct adhesions in filopodia: shaft adhesions control lamellar extension. J Neurosci 22(18):8071–8083

43. Thievessen I, Thompson PM, Berlemont S, Plevock KM, Plotnikov SV, Zemljic-Harpf A, Ross RS, Davidson MW, Danuser G, Campbell SL, Waterman CM (2013) Vinculin–actin interaction couples actin retrograde flow to focal adhesions, but is dispensable for focal adhesion growth. J Cell Biol 202(1):163–177. doi:10.1083/jcb.201303129

44. Uyaver S, Hansmann UHE (2014) Multicanonical Monte Carlo simulations of a de novo designed protein with end-to-end β-sheet. J Chem Phys 140(6):065,101

45. Viet MH (2012) Numerical study of protein–ligand binding: implications for alzheimer's disease and influenza virus. Ph.D. thesis

46. Vogel V, Sheetz M (2006) Local force and geometry sensing regulate cell functions. Nat Rev Mol Cell Biol 7(4):265–275. doi:10.1038/nrm1890

47. Waisman H, Fish J (2008) A heterogeneous space - time full approximation storage multilevel method for molecular dynamics simulations. Int J Numer Methods Eng 73(3), 407–426

48. Wozniak MA, Chen CS (2009) Mechanotransduction in development: a growing role for contractility. Mol Cell Biol 10(1):34–43. doi:10.1038/nrm2592

49. Zamir E, Geiger B (2001) Molecular complexity and dynamics of cell–matrix adhesions. J Cell Sci 114(Pt 20):3583–3590

50. Zhang H, Berg JS, Li Z, Wang Y, Lång P, Sousa AD, Bhaskar A, Cheney RE, Strömblad S (2004) Myosin-X provides a motor-based link between integrins and the cytoskeleton. Nat Cell Biol 6(6):523–531. doi:10.1038/ncb1136